Hydrogen evolution on Au(111) covered with submonolayers of Pd

Mårten E. Björketun,[1,*] Gustav S. Karlberg,[1] Jan Rossmeisl,[1] Ib Chorkendorff,[2] Holger Wolfschmidt,[3] Ulrich Stimming,[3] and Jens K. Nørskov[1,4]

[1]*Center for Atomic-scale Materials Design, Department of Physics, Technical University of Denmark, DK-2800 Lyngby, Denmark*
[2]*Center for Individual Nanoparticle Functionality, Department of Physics, Technical University of Denmark, DK-2800 Lyngby, Denmark*
[3]*Department of Physics E19, Technische Universität München, James-Franck-Str.1, D-85748 Garching, Germany*
[4]*SUNCAT Center for Interface Science and Catalysis, SLAC National Accelerator Laboratory, 2575 Sand Hill Road, Menlo Park, California 94025, USA and Department of Chemical Engineering, Stanford University, Stanford, CA 94305, USA*

(Received 7 March 2011; revised manuscript received 12 May 2011; published 5 July 2011)

A theoretical investigation of electrochemical hydrogen evolution on Au(111) covered with submonolayers of Pd is presented. The size and shape of monoatomically high Pd islands formed on the Au(111) surface are determined using Monte Carlo simulations, for Pd coverages varying from 0.02 to 0.95 ML. The energetics of adsorption and desorption of hydrogen on/from different types of sites on the Pd-Au(111) surface are assessed by means of density functional theory calculations combined with thermodynamic modeling. Based on the density functional and Monte Carlo data, the hydrogen evolution activity is evaluated with a micro-kinetic model. The analysis reproduces measured Pd-coverage-dependent activities for Pd submonolayers exceeding ∼0.15 ML and enables the relative contributions from different types of electrocatalytically active sites to be determined. Finally, the implications of surface line defects for Pd island formation and hydrogen evolution are discussed. It is argued, with support from theoretical data, that this kind of defects is likely to be responsible for a dramatic increase in activity observed experimentally [ChemPhysChem **7**, 985 (2006); Electrochim. Acta **52**, 5548 (2007)] at low Pd coverages.

DOI: 10.1103/PhysRevB.84.045407 PACS number(s): 68.43.Bc, 68.47.De, 82.45.Jn

I. INTRODUCTION

Careful experimental investigations of simple reactions on well defined surfaces are instrumental in revealing the underlying basic relations between surface structure and activity/selectivity.[1–13] To further the understanding, the experimental endeavors may be combined or complemented with atomic-scale simulations which have recently provided valuable information on catalytic reactions on elemental metal and metal alloy surfaces[14] and been used to design new electrocatalysts.[15,16]

The AuPd system is one of the more extensively studied bimetallic model electrocatalysts. It has been tested for a range of electrochemical reactions[1] and has attracted special attention for its ability to catalyze the hydrogen evolution reaction (HER).[1,2,4,17,18] Its catalytic activity can be varied substantially by modification of the structure and composition of the surface. Accordingly, the literature contains numerous records of AuPd surface alloys[5,19,20] and of Pd nanoparticles,[21,22] submonolayers,[2–4,17,23] and mono- and multilayers[1,24–30] deposited on well defined Au single crystal surfaces.

Thanks to the combined experimental and theoretical efforts the chemistry of the HER now appears to be well understood in the multilayer regime, as suggested by the excellent agreement between theoretical predictions[24,25] and experimental measurements[1,13] of the hydrogen evolution rate versus thickness of the Pd overlayer. Significant advances have also been made in the understanding of the Pd nanoparticles. Atomic-scale simulations have shown that small Pd clusters on Au generally interact less strongly with adsorbates (including hydrogen) than the corresponding pseudomorphic Pd overlayers.[22] Furthermore, a joint experimental and theoretical work has demonstrated a thickness-dependent variation in activity of the Pd nanoparticles, caused by a variation in the support-induced strain at the surface of the Pd nanoparticles.[21] Finally, hydrogen evolution rates have also been measured on Au(111) covered with monoatomically thick submonolayers of Pd.[2,17] These works report a dramatic increase in total activity as the Pd coverage is reduced to small fractions of a monolayer. This remarkable effect has been difficult to explain with any of the known catalytic properties of the Pd-Au(111) surface, but it indicates that some specific, highly active, AuPd environment abounds in the low coverage regime.

Inspired by the two latter experimental works,[2,17] this paper will focus on the less well understood Pd submonolayer regime. Special attention will be paid to the HER activity of different Pd-Au sites and the surprisingly high activity at small Pd submonolayers. The following approach is adopted: to start with, first-principle (FP) techniques are used to investigate the energetics of adsorption and desorption of hydrogen from a large number of different types of sites on the Pd submonolayer-Au(111) surface. Next, the structure and size distribution of Pd islands formed on the Au(111) surface are determined by means of Monte Carlo (MC) simulations. The FP and MC results are then used in conjunction with a micro-kinetic model to assess the hydrogen evolution activity of Pd-Au(111) surfaces for a wide range of Pd submonolayer coverages. This qualitatively reproduces the measured activity/Pd-coverage relation for all but the lowest parts of the submonolayer regime. Finally, in a set of elegant experiments Hernandez and Baltruschat have shown that Pd-decorated Au line defects are very efficient in catalyzing the HER.[4] In this work these types of defects are investigated in some detail and based on FP data it is shown that they might be responsible for the intriguing increase in HER activity at low Pd coverages.

II. THEORETICAL MODELING

A. Monte-Carlo simulations

The formation of monoatomically high Pd islands on Au(111), at 300 K, is investigated using Metropolis MC simulations. Starting from a random distribution of Pd atoms, corresponding to a certain Pd coverage θ_{Pd}, the islands evolve on a 100×100 hexagonal lattice subject to periodic boundary conditions. The total energy of the system is calculated as $E_{\mathrm{tot}} = N \times E_{\mathrm{b}}$, where N is the number of Pd-Pd bonds and $E_{\mathrm{b}} < 0$ is the Pd-Pd bond energy. If the displacement of a Pd atom from one lattice site to a neighboring site either reduces the total energy or leaves it unchanged, *i.e.* the change in energy from step t to step $t+1$

$$\Delta E = (N_{t+1} - N_t) \times E_{\mathrm{b}} \leqslant 0, \tag{1}$$

that process will be immediately accepted. If, on the other hand, the total energy increases as a result of the displacement, it can still occur but only with a probability of $\exp(-\Delta E/k_{\mathrm{B}}T)$.

B. Micro-kinetic and thermodynamic modeling

The total HER, $2(\mathrm{H}^+ + \mathrm{e}^-) \rightarrow \mathrm{H}_2$, taking place at an electrode in contact with an electrolyte involves three elementary reaction steps. In the initial step, the Volmer reaction, a proton from the electrolyte is adsorbed on the electrode to form atomic hydrogen, according to $\mathrm{H}^+ + \mathrm{e}^- \rightarrow \mathrm{H}^*$. This process is usually considered to be fast.[31] The subsequent hydrogen evolution can be accomplished either by the Tafel reaction, $2\mathrm{H}^* \rightarrow \mathrm{H}_2$ (recombination of two atomically adsorbed hydrogen), or the Heyrovsky reaction, $\mathrm{H}^* + \mathrm{H}^+ + \mathrm{e}^- \rightarrow \mathrm{H}_2$ (recombination of an atomically adsorbed hydrogen with a proton from the electrolyte and an electron provided by the electrode). Recent theoretical work[32,33] has indicated that the Volmer-Tafel channel is totally dominating for potentials close to zero on the normal hydrogen electrode (NHE) scale. Hence, the Heyrovsky reaction can be ignored at small overpotentials.

Taking only the Tafel pathway into account, the average rate of hydrogen desorption from sites of type i (i can be for instance fcc sites on the Au substrate and on the Pd islands or low-coordinated sites on the rims of the Pd islands) is given by

$$r_{\mathrm{des}}^{i} = \nu \theta_{\mathrm{H}^*,i}^2 \exp\left(-E_i^{\mathrm{Ta}}/k_{\mathrm{B}}T\right). \tag{2}$$

Here ν is an attempt frequency, henceforth assumed to be materials independent ($\nu = 10^{13}\ \mathrm{site}^{-1}\mathrm{s}^{-1}$), $\theta_{\mathrm{H}^*,i}$ the hydrogen coverage on sites i, and E_i^{Ta} the corresponding Tafel barrier. The latter two quantities depend on the applied electrode potential U. Alternatively, if hydrogen atoms from sites i recombine with hydrogen atoms from sites j, the desorption rate is instead given by

$$r_{\mathrm{des}}^{ij} = \nu \theta_{\mathrm{H}^*,i} \theta_{\mathrm{H}^*,j} \exp\left(-E_{ij}^{\mathrm{Ta}}/k_{\mathrm{B}}T\right). \tag{3}$$

Continuing from Eq. (2), the total desorption rate from an area equal to N_{tot} atoms can be expressed as

$$r_{\mathrm{des}}^{\mathrm{tot}} = \nu \sum_i N_i \theta_{\mathrm{H}^*,i}^2 \exp\left(-E_i^{\mathrm{Ta}}/k_{\mathrm{B}}T\right), \tag{4}$$

where N_i is the number of sites of type i on this area. It should be noted that $\sum_i N_i$ does not have to equal N_{tot}; a certain surface metal may provide more or less than one desorption site. Finally, when the area from which the desorption is measured is given by N_{tot} Au atoms, the rate $r_{\mathrm{des}}^{\mathrm{tot}}$ ($\mathrm{site}^{-1}\mathrm{s}^{-1}$) evaluated at $U = 0$ can be converted to exchange current density j_0 (Acm^{-2}) by multiplying Eq. (4) with $4.16 \times 10^{-4}/N_{\mathrm{tot}}$, yielding

$$j_0 = 4.16 \times 10^{-4} \frac{\nu}{N_{\mathrm{tot}}} \sum_i N_i \theta_{\mathrm{H}^*,i}^2 \exp\left(-E_i^{\mathrm{Ta}}/k_{\mathrm{B}}T\right). \tag{5}$$

Both θ_{H^*} and E^{Ta} in Eqs. (2)–(5) are intimately related with the standard free energy of hydrogen adsorption, ΔG_0, as we will see in the following.

The equilibrium H coverage on the surface at a potential U is given by the following condition for the differential free energy of H adsorption:[34]

$$\Delta G(\theta_{\mathrm{H}^*}^{\mathrm{eq}}, U) = \Delta G_0 - T\Delta S_{\mathrm{conf}} + eU = 0. \tag{6}$$

ΔG_0 is the reaction free energy for $1/2\mathrm{H}_2 \rightarrow \mathrm{H}^*$ at standard conditions ($\mathrm{pH} = 0$, $p_{\mathrm{H}_2} = 1$ bar, $T = 298$ K). It can be computed using FP calculations and standard molecular tables via the expression

$$\Delta G_0 = \Delta E + \Delta ZPE - T\Delta S. \tag{7}$$

Here ΔE is the coverage-dependent differential adsorption energy and ΔZPE the difference in zero point energy for the above reaction, both given by FP calculations. ΔS is the difference in entropy, which includes the loss in translational degrees of freedom during adsorption (taken from standard tables) as well as the vibrational entropy of the adsorbed state as given by FP calculations. At standard conditions ΔZPE and $-T\Delta S$ add up to a total of $\sim$0.24 eV on most metals,[35] a value that has been assumed in all calculations of the free energy in this work. Finally, ΔS_{conf} in Eq. (6) is the differential configurational entropy of non-interacting particles,

$$\Delta S_{\mathrm{conf}} = k_{\mathrm{B}} \ln\left(\frac{1-\theta_{\mathrm{H}^*}}{\theta_{\mathrm{H}^*}}\right). \tag{8}$$

The equilibrium hydrogen coverage is solved for by combining Eqs. (6) and (8), giving

$$\theta_{\mathrm{H}^*}^{\mathrm{eq}}(U) = \frac{1}{1 + \exp[(\Delta G_0 + eU)/k_{\mathrm{B}}T]}. \tag{9}$$

Furthermore, according to the barrier calculations performed in Ref. 33 the activation energies for H desorption from metal and metal alloy (111) surfaces via the Tafel mechanism obey the Brønsted-Evans-Polanyi relation

$$E^{\mathrm{Ta}} = 0.77 - 0.90\Delta G_0\,\mathrm{eV}, \tag{10}$$

with ΔG_0 defined as in Eq. (7). In principle, ΔG_0 exhibits a certain coverage dependance and consequently also varies with applied potential. However, within the experimentally relevant potential regime this variation is negligible for the surfaces considered here. Consequently, as seen by inspection of Eqs. (9) and (10), only the hydrogen adsorption energy ΔE has to be calculated in order to evaluate $\theta_{\mathrm{H}^*,i}$ and E_i^{Ta}.

C. Density functional theory details

Standard free energies of hydrogen adsorption, ΔG_0, and Pd-Pd bond energies are evaluated using first-principles calculations. The first-principles calculations are carried out within the framework of density functional theory (DFT) using the plane-wave[36,37] pseodopotential approach, as implemented in the DACAPO code.[38] For the exchange-correlation part the Revised-Perdew-Burke-Ernzerhof (RPBE)[39] version of the generalized gradient approximation is employed. The ion cores are described by ultrasoft pseudopotentials,[40] and for the expansion of the one-electron wave functions an energy cutoff of 340 Ry is used in all calculations. The Brillouin-zone is sampled using a $4 \times 4 \times 1$ Monkhorst-Pack k-point mesh for the smallest, 2×2, Au(111) surface cells and for larger surface cells the k-point mesh is reduced accordingly. A four atom wide Au(211) surface is used to model Au steps and in this case a $2 \times 4 \times 1$ k-point mesh is used. To improve the convergence of the Fermi discontinuity the Kohn-Sham states are smeared according to a Fermi-Dirac distribution with a smearing parameter $k_B T = 0.1$ eV. All total energies are subsequently extrapolated to $k_B T = 0$ eV.

For the Tafel reaction and H adsorption it has been shown that the reaction energies and activation energies are almost unaffected by water, electric potentials and electric fields.[34,41] This is not surprising since no electrons are transferred during this reaction and the dipole of the adsorbed H is small in the direction perpendicular to the surface. Hence, these effects can be neglected and only a surface slab and adsorbed hydrogen have to be included in the atomic model. Consequently, the surfaces are modeled using periodically repeated slab supercells, without water, varying in thickness from three to four layers (depending on Pd coverage) and in lateral extension from 2×2 to 4×4 primitive surface cells. A vacuum of $14 - 16$ Å is separating neighboring supercells in the z-direction. H is adsorbed on one of the two surfaces of the slab and the dipole correction[42] is used to decouple the interaction between periodically repeated slabs. Structural relaxations are performed with the two bottom layers of the slab hold fixed at the RPBE lattice constant of Au (4.22 Å), while the remaining atoms are allowed to adjust until the magnitudes of all residual forces are less than 0.01 eV/Å.

III. RESULTS AND DISCUSSION

A. Hydrogen adsorption

As an initial step in the analysis of the HER, ΔG_0 is calculated on Au(111), on Pd ensembles embedded in the Au(111) matrix and on Pd islands of various sizes. The most relevant adsorption sites are indicated in Fig. 1 and the corresponding adsorption energies as given by DFT are reported in Table I. The adsorption is highly endothermic on Au(111), on Pd monomers in the Au(111) matrix and on Pd_1 islands, while it is highly exothermic on the terraces of the larger Pd islands (Pd_n, $n \geqslant 3$). On the other hand, the rims of the larger Pd islands as well as Pd dimers and trimers in the Au(111) matrix provide adsorption sites with $\Delta G_0 \approx 0$ eV. These ΔG_0 values are close to optimal for the HER, which

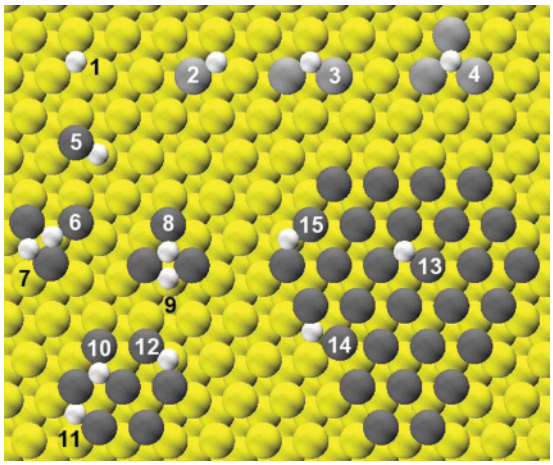

FIG. 1. (Color online) Adsorption sites for H on the Pd-Au(111) surface. The cartoon shows the most relevant adsorption sites on (1) Au(111), on Pd (2) monomers, (3) dimers and (4) trimers embedded in the Au matrix, and on (5) Pd_1, (6-9) Pd_3, (10-12) Pd_7 and (13-15) Pd_n islands.

can be seen by combining Eqs. (2), (9) and (10) at $U = 0$, giving

$$r_{\mathrm{des}} = \nu \times \frac{\exp(-(0.77 - 0.90\Delta G_0)/k_B T)}{[1 + \exp(\Delta G_0/k_B T)]^2}, \qquad (11)$$

and then differentiating the expression with respect to ΔG_0. It should be noted, though, that H is more strongly adsorbed on larger Pd ensembles in Au(111); e.g., $\Delta G_0 = -0.17$ eV on a Pd_7 ensemble and on very large ensembles ΔG_0 is expected to approach -0.32 eV, the adsorption energy on a pseudomorphically grown Pd overlayer on Au(111).

The observation that hydrogen adsorption is weak on Pd monomers but much closer to the optimum on dimers and trimers is consistent with the experimental finding by Maroun *et al.* who conclude that hydrogen adsorption requires at least

TABLE I. Adsorption free energy of H on terrace and rim sites and on ensembles embedded in the Au matrix. With one exception, the adsorption sites are indicated in Fig. 1.

Surface nano-structure	H adsorption site	ΔG_0 (eV)
Au(111)	1	0.33
Pd monomer	2	0.26
Pd dimer	3	0.07
Pd trimer	4	−0.13
Pd_7 ensemble		−0.17
Pd_1 island	5	0.20
Pd_3 island	6	−0.22
	7	0.11
	8	−0.31
	9	0.20
Pd_7 island	10	−0.26
	11	−0.05
	12	0.05
Pd_n island	13	−0.27
	14	−0.05
	15	0.20

Pd dimers.[5] Moreover, the strong adsorption on the terrace of Pd_3 (−0.31 eV), comparable to that of the pseudomorphically grown Pd overlayer on Au(111), and the weaker adsorption (−0.26 eV) on the bigger Pd_7 island is consistent with the calculated hydrogen binding energies reported by Roudgar and Gross.[22] The good agreement with previously published data gives us confidence in the calculated adsorption energies.

B. Surface nano-structure

Next, the formation of Pd islands on Au(111) is investigated using MC simulations. These simulations require as input the strength of the pair interaction (bond energy) between Pd atoms in the islands. Together with the temperature and the initial Pd distribution, this parameter will determine the evolution of the system. The average bond energy (Pd-Pd bond) in an island consisting of n Pd atoms (Pd_n), deposited on an Au(111) substrate, is evaluated according to

$$E_b = (E_{Pd_n} + (n-1)E_{Au(111)} - nE_{Pd_1})/m, \qquad (12)$$

where $E_{Au(111)}$ is the energy of a pure Au slab, E_{Pd_n} the energy of an Au slab with Pd_n deposited on top, E_{Pd_1} the energy of an Au slab with a single Pd on top, and, finally, m the number of Pd-Pd bonds in Pd_n. The reference system is thus n isolated Pd adsorbed on the Au surface. Based on DFT calculations the average bond energies are estimated to −0.20 eV for Pd_2, Pd_3 and Pd_4, to −0.21 eV for Pd_7, and to −0.22 eV for a full Pd monolayer. As the difference in bond energies between the smallest islands and the full monolayer is minute, the bond energy is approximated with −0.20 eV (per Pd-Pd bond) for all island sizes in the MC simulations.

As an illustration, the evolution of the $\theta_{Pd} = 0.2$ monolayer (ML) system is traced in Fig. 2(a)–2(c); the real-space Pd distributions (upper panels) and corresponding island perimeter distributions are reported after 1×10^4, 1×10^6 and 1×10^8 steps. The initial phase (of the order 10^5 steps) is characterized by rapid expansion of the islands as isolated Pd atoms start to merge, forming more stable entities. After this brief initial period the islands continue to grow but at a much more moderate rate. In order for an island to grow it must now either attract a single Pd atom that has first escaped from an other island, which is a very rare event, or it can merge with an entire, slowly migrating, island. Due to the expansion of the islands, the ratio of active rim sites to less active terrace sites will gradually decrease, resulting in a reduced overall contribution from the islands to the HER. A similar continuous growth of Pd islands with time is observed experimentally as demonstrated by Fig. 2(d)–2(f), which contains a series of images of growing Pd islands measured by *in situ* scanning tunneling microscopy (STM). It should be noted, though, that the simulated and measured evolutions reported here are not directly comparable since neither the time scale (kinetic barriers would have to be included in the MC model in order to introduce a proper time coordinate in the simulations) nor the Pd coverage is the same.

The last snapshot from the simulation, Fig. 2(c), taken after 1×10^8 steps, a point at which the growth has become very slow, might be compared with the distribution of Pd electrodeposited on Au as measured by Pandelov and Stimming using *in situ* STM.[2] Compared to our simulated distribution, the distribution measured for $\theta_{Pd} = 0.23$ ML is shifted to larger perimeters; it is centered at ∼7 nm and has a longer tail toward large perimeters. Our distribution is in better agreement with the one measured for $\theta_{Pd} = 0.09$ ML. One reason for the discrepancy between the experimental and modeled cluster sizes is the arbitrariness of the comparison. For example, the equilibration of the experimental system at the point of measurement is unknown and longer MC simulations would obviously shift the distribution toward larger perimeters. In addition to this, the simple MC model used here has some intrinsic limitations that further complicate comparison with experimental results. Firstly, the assumption that the Pd-Pd bond energy is always approximately −0.20 eV was based on calculations on either small Pd islands or a full Pd monolayer. None of these systems contain four- or five-fold coordinated Pd atoms. Taking such configurations into consideration could potentially affect the assumption. Secondly, only nearest neighbor Pd-Pd interactions are accounted for although interactions beyond nearest neighbors might also influence the growth of the islands. Thirdly, no kinetic barriers are included in the model and hence it is impossible to establish a proper time scale for the evolution of the islands. Obviously, a more quantitative comparison with experiments would call for a model that contains all these details.[43] However, as will be shown in Sec. III D, for our purpose of providing a qualitative understanding of the Pd coverage dependent HER activity a good agreement with measured cluster sizes is not required.

Before analyzing the HER activity, we will briefly discuss two other aspects of the surface structure and surface composition. First, we consider the potential formation of Pd ensembles embedded in the Au(111) surface under electrochemical conditions. Interactions between Pd atoms in these ensembles can be estimated in a fashion similar to that used above to calculate bond energies between Pd atoms in Pd islands. By comparing DFT energies of ensembles on one hand and of monomers on the other, it is concluded that the interactions are repulsive; it costs 0.19 eV to form a dimer from two isolated monomers and 0.19 − 0.24 eV to form a trimer from an isolated monomer and an isolated dimer depending on the structure of the trimer. This result compares well with the Pd ensemble distribution reported by Maroun *et al.* for atomically flat PdAu(111), prepared by electrodeposition of Pd on Au(111).[5] Using atomic resolution *in situ* STM, they found an overrepresentation of monomers and an underrepresentation of dimers and trimers, as compared with random distributions, in Pd_7Au_{93} and $Pd_{15}Au_{85}$. That monomers will be favored was later shown also by Yuan *et al.* based on DFT calculations.[20] Since Pd atoms tend to repel each other and H adsorption on monomers is highly endothermic, we do not expect surface embedded Pd to contribute much to the HER at low Pd concentrations ($\theta_{Pd} \lesssim 0.2$). At higher concentrations one might force the formation of dimers and trimers (and also larger ensembles, but those are less active). However, at these Pd concentrations the active island rim sites will be much more abundant and dominate the HER. Au-embedded Pd ensembles will therefore be excluded from the analysis of the electrocatalytic activity.

Secondly, we investigate how monoatomic high Au steps, which will doubtlessly be present on any flat Au surface, affect

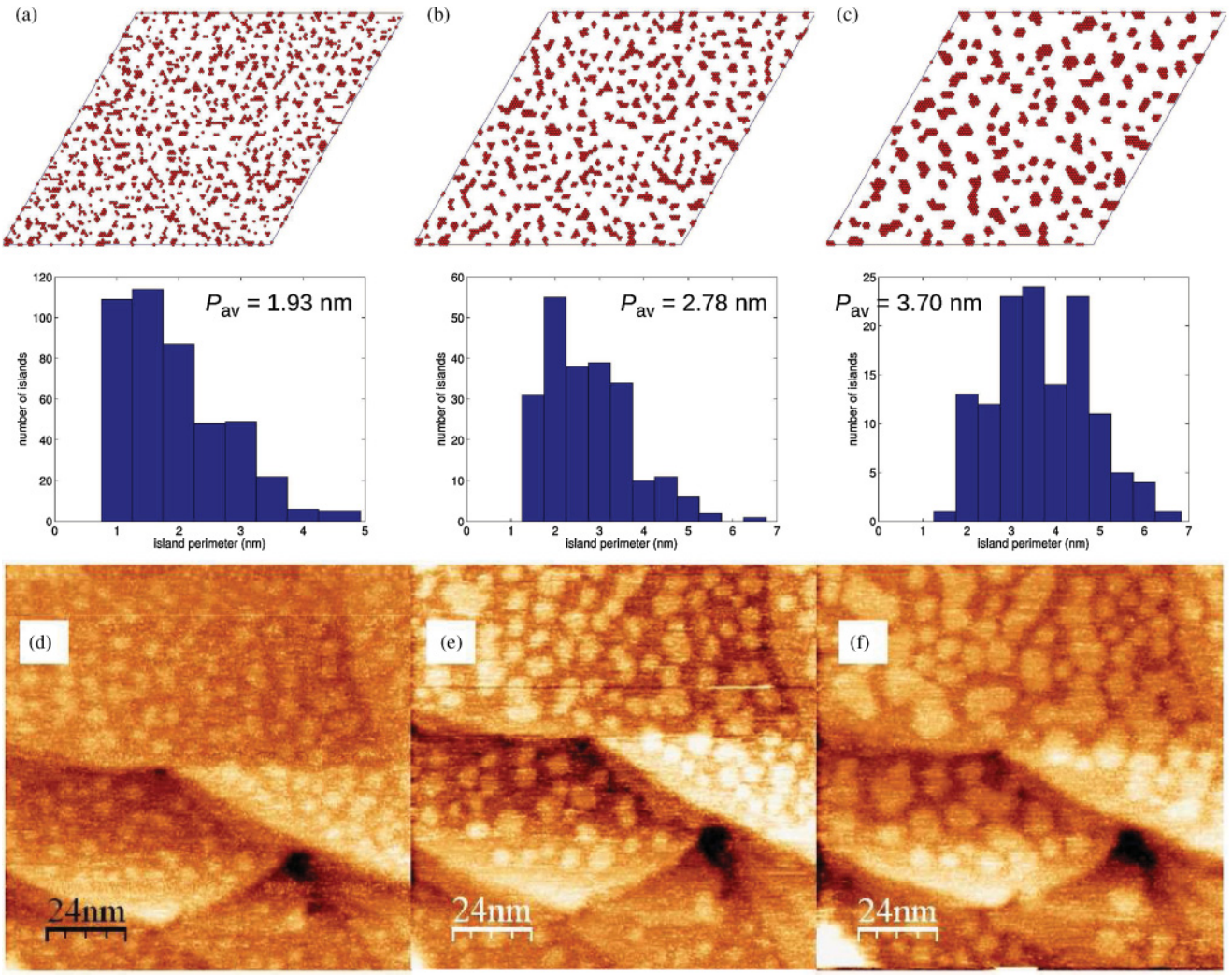

FIG. 2. (Color online) (a-c) Simulated formation of Pd islands on Au(111). The Pd coverage is 0.2 ML and the Pd atoms interact attractively with an energy of 0.20 eV per Pd-Pd bond. The snapshots are taken after (a) 1×10^4, (b) 1×10^6, and (c) 1×10^8 steps in the simulation. The upper panels show the real-space Pd distribution and the lower panels show the corresponding distributions of island perimeters, obtained by assuming that all islands adopt a circular shape. (d-f) *In situ* measurements of Pd growth on Au(111) in 0.1 M HSO_4+ 0.1 mM $PdSO_4$; $U_{W_e} = 700$ mV *vs.* NHE, $U_{tip} = 900$ mV *vs.* NHE, $I_{tun} = 1$ nA. The time scale from image (d) to (e) and from image (e) to (f) is about 5 min, details are given in Ref. 3.

the growth of Pd layers. In a recent publication, Köntje *et al.* reported that perfectly flat Au terraces transform into terraces partially covered with monoatomic high Au islands at potentials lower than the onset potential of Pd electrodeposition.[44] Accordingly, the density of Au steps can be expected to be relatively high at the conditions under which the Pd films are grown. The authors also pointed out that Pd deposition always starts at the Au edges, unless high overpotentials are applied, which facilitate deposition also on terraces. The same conclusion was also drawn by Hernandez and Baltruschat from experiments on well characterized stepped Au surfaces.[23] The notion that Pd layers start to grow from Au edges is supported by our DFT calculations, estimating the adsorption of a single Pd to be ∼0.5 eV stronger at the edge than on the terrace (c.f. Fig. 3). The DFT calculations further indicate that Pd atoms deposited at the edge tend to cluster due to the energy gained by formation of additional bonds and that it is energetically favorable to fill all edge sites before starting to populate adjacent terrace sites. This growth pattern has implications for the HER at small Pd coverages, an issue we will return to at the end of next section.

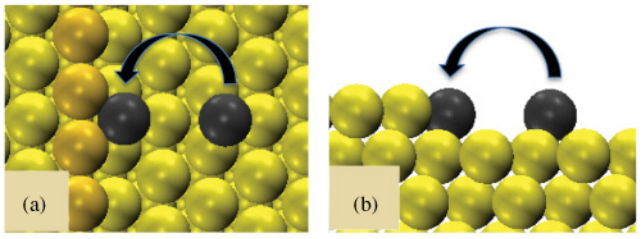

FIG. 3. (Color online) (a) Top and (b) side view of isolated Pd atoms adsorbed on a stepped Au surface. The Pd atom is stabilized with approximately 0.5 eV when moved from the close packed terrace to the edge.

C. Electrocatalytic hydrogen evolution activity

When estimating the electrocatalytic HER activity, we first consider desorption only from fcc sites on the bare Au(111) surface and from the rims and terraces of the Pd islands, while possible contributions from Pd ensembles in the Au(111) surface and from Pd atoms at Au edges are ignored. We assume that the Pd islands are all fairly large with adsorption properties similar to those of Pd_n (this should be a reasonable approximation except for the earliest stages of the island evolution) and thus take ΔG_0 to be 0.33 eV on Au(111), −0.27 eV on Pd terraces, and −0.05 eV and 0.20 eV on strongly and weakly adsorbing Pd rim sites, respectively. These standard free energies will determine the hydrogen occupancies, $\theta_{H^*}^{eq}(U)$, of the different sites at a given potential according to Eq. (9). We further assume that H adsorbed on Au(111) and on Pd terraces desorb by recombining with like H, that strongly adsorbed H on Pd rims desorb by recombining with H from the Pd terrace and that an H weakly adsorbed on a Pd rim desorbs by recombining with an H strongly adsorbed on the rim. These assumptions, combined with Eq. (10), give Tafel activation energies, E^{Ta}, of 0.47, 1.00, 0.90 and 0.69 eV, respectively, for the four desorption processes. Once an island formation simulation for a certain θ_{Pd} has reached a stage characterized by very slow growth of the islands (which it has after 1×10^8 steps), the number of Pd terrace and rim sites are counted and the exchange current of that system is calculated by means of Eq. (5) based on the $\theta_{H^*}^{eq}$ and E^{Ta} specified above.

Figure 4 shows the calculated HER activity, in terms of the exchange current j_0, plotted as a function of Pd coverage ($0.02 \leqslant \theta_{Pd} \leqslant 0.95$ ML). Apart from the total activity, the figure also reports the individual contributions from Au(111), Pd terraces and Pd rims. The combined contribution from Au(111) and Pd terraces, j_0^{Au+Pd}, follows closely the linear interpolation between Au(111) and 1ML Pd/Au(111) that would be expected for the total activity if HER occurred predominantly on Pd terraces. It is clear, however, that the Pd rims give the paramount contribution, except on surfaces with Pd coverages close to 1 (at $\theta_{Pd} = 1$ ML there are only Pd terrace sites available). The importance of the rim sites has previously been emphasized by Kibler based on a combination of electrochemical and *in situ* STM measurements.[17,45] Over most of the coverage range ($\theta_{Pd} > 0.15$ ML) the total-activity curve is rather flat, a prediction that agrees fairly well with exchange current data reported by Kibler.[17] The rates are roughly the same for $\theta_{Pd} = 0.15$ ML and $\theta_{Pd} = 0.95$ ML and the maximum rate, at $\theta_{Pd} \approx 0.6$ ML, is approximately twice as high. This shape is not surprising given that the HER takes place predominantly on the rims, a similarly shaped total-activity curve can be deduced from a very simple cluster model: Let us assume that for Pd coverages below 0.5 ML the simulation cell will contain a single circular island in the thermodynamic limit and likewise a single circular hole will be formed in the Pd layer for Pd coverages exceeding 0.5 ML. The number of rim sites will then be proportional to $\theta_{Pd}^{1/2}$ for $\theta_{Pd} < 0.5$ ML, proportional to $(1 - \theta_{Pd})^{1/2}$ for $\theta_{Pd} > 0.5$ ML and the maximum will occur at $\theta_{Pd} = 0.5$ ML. In this model the activity has dropped to half maximum at $\theta_{Pd} = 0.125$ ML and $\theta_{Pd} = 0.875$ ML. Compared to this simple model our simulated parabola is shifted to somewhat higher θ_{Pd}, but apart from that it is very similar.

At low coverages, $\theta_{Pd} < 0.1$, the total rate drops dramatically due to a rapid decrease in the number of rim sites. This drop is at variance with experimental findings. Kibler instead observed a remarkable increase in exchange current at low sub-monolayer coverages.[17] As pointed out in Ref. 17, another type of adsorption site, so far not included in our model, must be responsible for this curious behavior. An increase at low coverages was also noticed by Pandelov and Stimming in Pd-coverage dependent HER current densities measured at $U = -0.1$ and -0.2 V.[2] We can compare our data also with these measurements by generating Tafel plots, presented in Fig. 5, for a set of systems with θ_{Pd} varying from 0.02 to 0.95 ML. These curves are obtained by introducing a potential dependence in Eq. (5), through θ_{H^*}, and subtracting the corresponding hydrogen oxidation current. As expected, $\theta_{Pd} = 0.6$ ML is the most active system at small overpotentials,

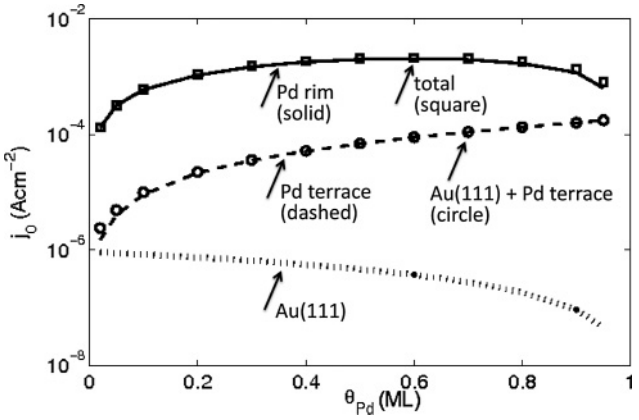

FIG. 4. Hydrogen evolution exchange current (squares) on Pd-Au(111) as a function of Pd coverage. The exchange current has been calculated after 1×10^8 steps for systems where the attractive Pd-Pd interaction is 0.20 eV. The individual contributions to the exchange current from the Au surface (dotted line), Pd island terraces (dashed line), and Pd island rims (solid line) are also indicated.

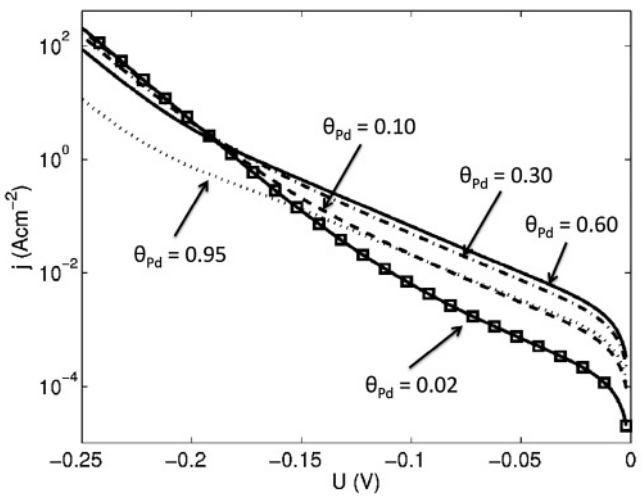

FIG. 5. Tafel plots of hydrogen evolution on Au(111) covered with different amounts of Pd.

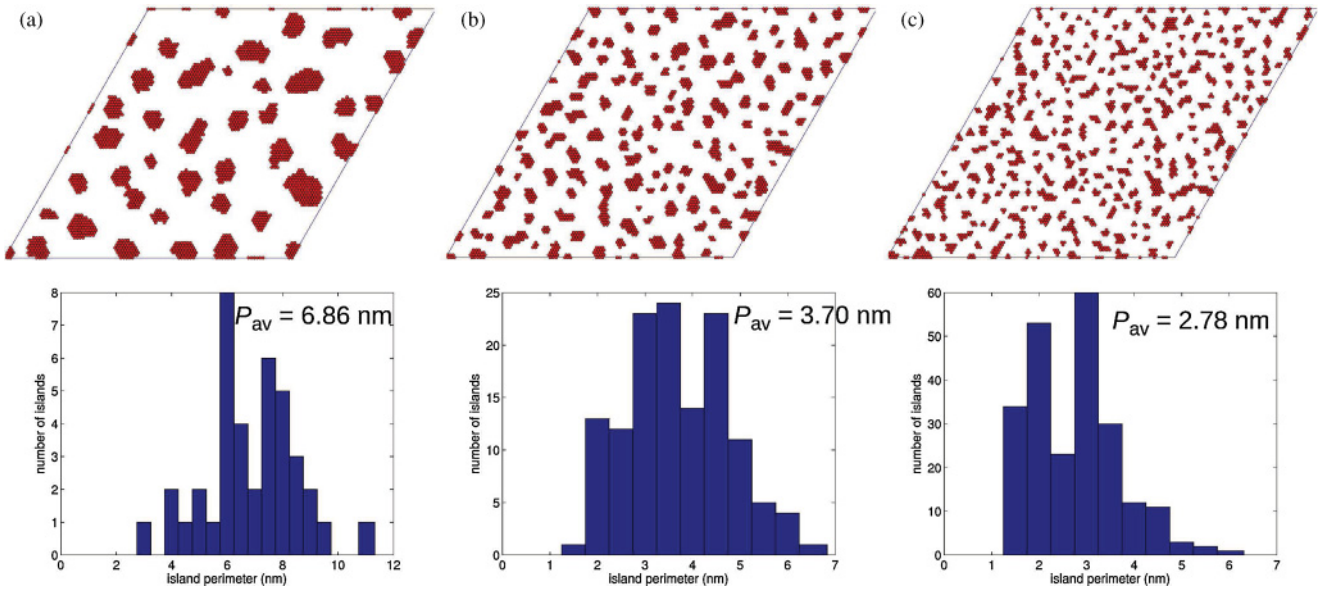

FIG. 6. (Color online) Simulated formation of Pd islands on Au(111). The snapshots are taken after 1×10^8 steps. The Pd coverage is 0.2 ML and the Pd atoms interact attractively with an energy of (a) 0.10 eV, (b) 0.20 eV, and (c) 0.40 eV per Pd-Pd bond. The upper panels show the real-space Pd distribution and the lower panels show the corresponding distributions of island perimeters, obtained by assuming that all islands adopt a circular shape.

but when more negative potentials are applied the gap between $\theta_{Pd} = 0.6$ ML and the low-coverage system $\theta_{Pd} = 0.02$ ML is gradually reduced until, eventually, at $U = -0.19$ V, $\theta_{Pd} = 0.02$ ML becomes most active. In passing, we note that the $\theta_{Pd} = 0.6$ ML system has a Tafel slope of 61 mV dec^{-1} in the potential range $-0.15 \leqslant U \leqslant -0.05$ V, which is comparable to the slope of 82 mV dec^{-1} for Pt(111) in the same potential range.[3] The change in activity order among the systems with applied potential is caused by changes in the H adsorption energetics on Au(111). Negative potentials facilitate H adsorption on Au(111) making these sites more important, something that obviously favors the low coverage systems which contain large areas of bare Au. Nevertheless, this does not satisfactorily explain the high rate measured by Pandelov and Stimming for $\theta_{Pd} \lesssim 0.15$ ML and $U > -0.2$ V. In order to detect an increase in activity at small submonolayer Pd coverages, more negative potentials ($\lesssim -0.2$ V) have to be applied in our simulations than in their measurements and in addition to that the increase we observe is much less pronounced.

From the above comparisons with experimental data, we can conclude that another, so far neglected but highly active, type of site must dominate the hydrogen evolution at low Pd coverages. In the following, we will demonstrate, relying on complementary DFT calculations, that such sites can indeed be created in the vicinity of Au steps, thus suggesting that Au steps might be indirectly responsible for the impressive activity in this regime.

Calculations on a Pd-Au(211) surface show that the first rows of Pd atoms deposited along an Au step provide H adsorption sites with $\Delta G_0 = -0.01$ eV, which can be compared to $\Delta G_0 = -0.05$ eV for the most active sites on the rims of larger Pd islands (it should be noted that when two Pd rows cover the Au edge, hydrogen preferentially adsorbs in hollow sites between the two rows, but once these more strongly adsorbing sites have been filled the outer Pd row provides sites with $\Delta G_0 = -0.01$ eV). According to Eq. (10) this rather modest increase of 40 meV in ΔG_0 is expected to lower the activation energy for H desorption with ~40 meV, which would result in a few times higher desorption rate (per site) at room temperature.

Since Pd atoms under most conditions preferentially fill the Au edges before starting to occupy terraces, we would expect the total hydrogen evolution rate to increase almost linearly as more Pd atoms are deposited, up to the point where the edges are fully covered with Pd. The rate would then stay fairly constant for a while when the first few Pd rows are formed outside the Au edge. This picture is consistent with hydrogen evolution measurements by Hernandez and Baltruschat on Pd-modified Au(332) where they found a high constant rate from the first Pd rows deposited along the Au step.[4] An even higher rate was measured on a mechanically damaged sample, presumably containing more defects, which further emphasizes the importance of under-coordinated Pd at Au defects. However, soon further increase of the Pd loading will result in blocking of the highly active sites by new Pd atoms whose catalytic properties resemble those of Pd atoms at the rims of larger islands. Hence, the total rate would start to drop and continue doing so until all (or most) highly active sites have been blocked. Upon further growth of the Pd layer, the activity would start to increase again simply because more Pd rim sites are created.

In the experiments on Pd-covered Au(111)[2,17] the absolutely highest total hydrogen evolution rate is observed for Pd loadings of one or a few percent of a ML, presumably corresponding to the point where the Au edges have been fully covered with highly active Pd (i.e. the Au edges are covered with one or a few rows of Pd). Despite the high activity of these sites, the hydrogen evolution from the Au-Pd edge would not be able to match the evolution from the much

larger number of Pd rim sites present at a Pd coverage of about 0.6 ML unless the difference in per site desorption rate would be much larger than one order of magnitude. However, a two orders of magnitude difference would probably be large enough to reproduce the experimental features. In order to obtain such a difference in desorption rate at room temperature, the difference in activation energy needs to be ∼130 meV instead of ∼40 meV. That could easily be the case given the error bar of the present calculations.

Finally, we note that the reverse reaction, the hydrogen oxidation reaction (HOR), was investigated in detail in Ref. 3. A similar increase in the geometric current density over Pd/Au(111) when lowering the amount of active Pd catalyst was observed also for the HOR. This result for coverages smaller than one complete monolayer can be understood using the same arguments as those used above to explain the HER.

D. Pd-Pd interaction effects

Finally, we explore what possible implications deviations from the Pd-Pd interaction $E_b = -0.2$ eV could have for the results presented above. A change in E_b would inevitably affect the Pd clustering and consequently also the electrocatalytic activity of the system. Hence, as there is an uncertainty related to the DFT energies, it is important to check the sensitivity of our results with respect to variations in E_b. Figure 6 reports the Pd island formation on the $\theta_{Pd} = 0.2$ ML surface after 1×10^8 MC steps, assuming a Pd-Pd bond energy of -0.10, -0.20 and -0.40 eV, respectively. It is obvious that weaker bonding promotes the mobility of the Pd atoms, which leads to faster growth of the islands. For instance, the average perimeter length is almost doubled after 1×10^8 steps when the magnitude of the Pd-Pd bond energy is reduced from 0.20 to 0.10 eV; with the weaker interaction the average perimeter is 6.86 nm which, by chance, happens to be close to what was measured by Pandelov and Stimming[2] for $\theta_{Pd} = 0.23$ ML. It is plausible that the same island sizes would be obtained also in the two other simulations, were they only run long enough. However, as Fig. 7 indicates, the convergence is not all that crucial. The foremost consequence of an improved convergence is a more or less constant reduction of the fraction of rim sites to terrace sites over the entire θ_{Pd} range. This results in a rather moderate lowering of the activity curve while its qualitative shape remains unaffected. Hence it can be concluded that a moderate change in E_b would not affect any of the general conclusions drawn in previous sections.

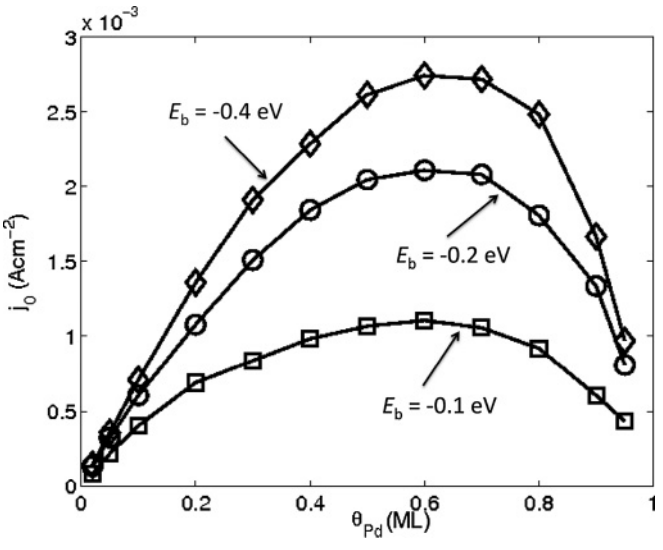

FIG. 7. Hydrogen evolution exchange current on Pd-Au(111) as a function of Pd coverage. The exchange current has been calculated after 1×10^8 steps for systems where the attractive Pd-Pd interaction is 0.10 eV (squares) 0.20 eV (circles), and 0.40 eV (diamonds).

IV. CONCLUSIONS

Based on density functional theory (DFT) calculations, the energetics of adsorption and desorption of hydrogen from different types of sites on the Pd submonolayer-Au(111) surface have been investigated. With respect to the criterion for an optimal hydrogen evolution catalyst ($\Delta G_0 \approx 0$ eV), hydrogen was found to be: (i) too strongly adsorbed on the terraces of Pd islands and on large Pd ensembles embedded in the Au(111) surface; (ii) too weakly adsorbed on Au(111), on single Pd atoms on top Au(111) and on Pd monomers embedded in Au(111); and (iii) close to optimally adsorbed on the rims of the Pd islands and on Pd dimers and trimers embedded in Au(111).

Moreover, based on Pd-Pd bond energies calculated by DFT, the shape and size distribution of Pd islands formed on the Au(111) surface have been determined by means of Monte Carlo simulations. The simulations reproduced experimental island distributions rather well, though on average the simulated islands are slightly smaller than their experimental counterparts. Probably the discrepancy originates from either overestimation of the Pd-Pd bond energy or too short Monte Carlo simulations. The equilibration of the experimental system at the point of measurement is unknown and longer Monte Carlo simulations would shift the distribution toward larger island areas.

The DFT and Monte Carlo results were then used in conjunction with a micro-kinetic model in order to assess the hydrogen evolution activity on Pd-Au(111) surfaces as a function of Pd coverage. This analysis successfully reproduced measured Pd-dependent activities for Pd submonolayers exceeding ∼0.15 ML and enabled the relative contributions from different types of electrocatalytically active sites to be determined.

Finally, the indirect effect of monoatomic high Au steps on the hydrogen evolution activity was investigated in some detail. With support from additional DFT data it was argued that these defects might be responsible for an experimentally observed dramatic increase in activity at low Pd coverages, an effect that could not be captured by theoretical modeling that took only data for perfectly flat Au substrates into account.

ACKNOWLEDGMENTS

The Center for Atomic-scale Materials Design is sponsored by the Lundbeck Foundation. Support from the Office of Science of the U.S. Department of Energy to the SUNCAT Center for Interface Science and Catalysis at SLAC/Stanford is gratefully acknowledged. We thank the Danish Center for Scientific Computing (DCSC) for financial support.

*martebjo@fysik.dtu.dk

[1] L. A. Kibler, Electrochim. Acta **53**, 6824 (2008).
[2] S. Pandelov and U. Stimming, Electrochim. Acta **52**, 5548 (2007).
[3] H. Wolfschmidt, R. Bußar, and U. Stimming, J. Phys. Condens. Matter **20**, 374127 (2008).
[4] F. Hernandez and H. Baltruschat, J. Solid State Electrochem. **11**, 877 (2007).
[5] F. Maroun, F. Ozanam, O. M. Magnussen, and R. J. Behm, Science **293**, 1811 (2001).
[6] V. R. Stamenkovic, B. Fowler, B. S. Mun, G. Wang, P. N. Ross, C. A. Lucas, and N. M. Markovic, Science **315**, 493 (2007).
[7] J. Zhang, M. B. Vukmirovic, Y. Xu, M. Mavrikakis, and R. R. Adzic, Angew. Chem. Int. Ed. **44**, 2132 (2005).
[8] R. R. Adzic, A. V. Tripkovic, and W. E. O'Grady, Nature **296**, 137 (1982).
[9] N. P. Lebedeva, M. T. M. Koper, E. Herrero, J. M. Feliu, and R. A. van Santen, J. Electroanal. Chem. **487**, 37 (2000).
[10] E. Herrero, J. M. Feliu, and A. Wieckowski, Langmuir **15**, 4944 (1999).
[11] W. Chrzanowski and A. Wieckowski, Langmuir **14**, 1967 (1998).
[12] M. Baldauf and D. M. Kolb, J. Phys. Chem. **100**, 11375 (1996).
[13] L. A. Kibler, A. M. El-Aziz, R. Hoyer, and D. M. Kolb, Angew. Chem. Int. Ed. **44**, 2080 (2005).
[14] J. K. Nørskov, T. Bligaard, J. Rossmeisl, and C. H. Christensen, Nature Chem. **1**, 37 (2009).
[15] J. Greeley, T. F. Jaramillo, J. Bonde, I. Chorkendorff, and J. K. Nørskov, Nat. Mater. **5**, 909 (2006).
[16] M. E. Björketun, A. S. Bondarenko, B. L. Abrams, I. Chorkenforff, and J. Rossmeisl, Phys. Chem. Chem. Phys. **12**, 10536 (2010).
[17] L. A. Kibler, ChemPhysChem **7**, 985 (2006).
[18] F. A. Al-Odail, A. Anastasopoulos, and B. E. Hayden, Phys. Chem. Chem. Phys. **12**, 11398 (2010).
[19] T. J. Schmidt, V. Stamenkovic, M. N. Markovic, and P. N. Ross, Electrochim. Acta **48**, 3823 (2003).
[20] D. Yuan, X. Gong, and R. Wu, Phys. Rev. B **75**, 085428 (2007).
[21] J. Meier, J. Schiøtz, P. Liu, J. K. Nørskov, and U. Stimming, Chem. Phys. Lett. **390**, 440 (2004).
[22] A. Roudgar and A. Groß, Surf. Sci. **559**, L180 (2004).
[23] F. Hernandez and H. Baltruschat, Langmuir **22**, 4877 (2006).
[24] A. Roudgar and A. Groß, Phys. Rev. B **67**, 033409 (2003).
[25] A. Roudgar and A. Groß, J. Electroanal. Chem. **548**, 121 (2003).
[26] H. Naohara, S. Ye, and K. Uosaki, J. Electroanal. Chem. **500**, 435 (2001).
[27] L. A. Kibler, M. Kleinert, R. Randler, and D. M. Kolb, Surf. Sci. **443**, 19 (1999).
[28] L. A. Kibler, M. Kleinert, and D. M. Kolb, Surf. Sci. **461**, 155 (2000).
[29] L. A. Kibler, M. Kleinert, V. Lazarescu, and D. M. Kolb, Surf. Sci. **498**, 175 (2002).
[30] E. Santos, P. Quaino, and W. Schmickler, Electrochim. Acta **55**, 4346 (2010).
[31] N. M. Markovic and P. N. Ross, Surf. Sci. Rep. **45**, 117 (2002).
[32] J. X. Wang, T. E. Springer, and R. R. Adzic, J. Electrochem. Soc. **153**, A1732 (2006).
[33] E. Skúlason, V. Tripkovic, M. E. Björketun, S. Gudmundsdóttir, G. S. Karlberg, J. Rossmeisl, T. Bligaard, H. Jónsson, and J. K. Nørskov, J. Phys. Chem. C **114**, 18182 (2010).
[34] G. S. Karlberg, T. F. Jaramillo, E. Skúlason, J. Rossmeisl, T. Bligaard, and J. K. Nørskov, Phys. Rev. Lett. **99**, 126101 (2007).
[35] J. K. Nørskov, T. Bligaard, A. Logadottir, J. R. Kitchin, J. G. Chen, S. Pandelov, and U. Stimming, J. Electrochem. Soc. **152**, J23 (2005).
[36] M. C. Payne, M. P. Teter, D. C. Allan, T. A. Arias, and J. D. Joannopoulos, Rev. Mod. Phys. **64**, 1045 (1992).
[37] G. Kresse and J. Furthmüller, J. Comput. Mater. Sci. **6**, 15 (1996).
[38] Dacapo pseudopotential code [https://wiki.fysik.dtu.dk/dacapo], Center for Atomic-scale Materials Design (CAMD), Technical University of Denmark, Lyngby.
[39] B. Hammer, L. B. Hansen, and J. K. Nørskov, Phys. Rev. B **59**, 7413 (1999).
[40] D. Vanderbilt, Phys. Rev. B **41**, 7892 (1990).
[41] E. Skúlason, G. S. Karlberg, J. Rossmeisl, T. Bligaard, J. Greeley, H. Jónsson, and J. K. Nørskov, Phys. Chem. Chem. Phys. **9**, 3241 (2007).
[42] L. Bengtsson, Phys. Rev. B **59**, 12301 (1999).
[43] Y. Han, B. Ünal, D. Jing, F. Qin, C. J. Jenks, D.-J. Liu, P. A. Thiel, and J. W. Evans, Phys. Rev. B **81**, 115462 (2010).
[44] C. Köntje, L. A. Kibler, and D. M. Kolb, Electrochim. Acta **54**, 3830 (2009).
[45] J. Tang, M. Petri, L. A. Kibler, and D. M. Kolb, Electrochim. Acta **51**, 125 (2005).